

Pore size distributions in nanoporous methyl silsesquioxane films as determined by small angle x-ray scattering

E. Huang,^{a)} M. F. Toney, W. Volksen, D. Mecerreyes, P. Brock, H.-C. Kim, C. J. Hawker, J. L. Hedrick, V. Y. Lee, T. Magbitang, and R. D. Miller
IBM Almaden Research Center, 650 Harry Road, San Jose, California 95120

L. B. Lurio

Department of Physics, Northern Illinois University, DeKalb, Illinois 60115

(Received 1 May 2002; accepted for publication 26 July 2002)

Small angle x-ray scattering (SAXS) measurements were performed on nanoporous methyl silsesquioxane films that were generated by the incorporation of a sacrificial polymeric component into the matrix and subsequently removed by thermolysis. The average pore radii ranged from 1 to 5 nm over a porosity range of ~5–50%. The distribution in pore size was relatively broad and increases in breadth with porosity. The values and observations obtained by SAXS are in good agreement with field emission scanning electron microscopy. © 2002 American Institute of Physics. [DOI: 10.1063/1.1507841]

As device dimensions in microprocessors shrink, signal delays and noise increase due to capacitive coupling and cross talk between metal interconnects. To minimize these effects, extensive effort has been directed toward replacing standard SiO₂ with new interlayer dielectrics having significantly lower dielectric constants, k . Nanoporous films provide a route to lowering the dielectric constant by substitution of a portion of the matrix material with air. Unlike early nanoporous organic dielectrics generated from diblock copolymers that microphase separated into discrete domains having a well defined size,¹ many of the nanoporous dielectrics of interest today are based on kinetically arrested phase separating systems where one component forms a rigid cross-linked network while the other is expelled from the film by thermolysis at elevated temperatures.² Methyl silsesquioxane (MSSQ)³ and cross-linked poly(arylenes),⁴ e.g., SiLKTM, are two materials currently being examined for the generation of nanoporous dielectrics. Due to the mechanism of phase separation however, these systems may exhibit a broader distribution in pore sizes.

One of the most important criteria for nanoporous films is that the pore size must be substantially smaller than device structures. For example, nanoporous films having pores comparable or larger than the pattern linewidth may lead to localized deformation or collapse due to insufficient structural support, formation of metal shorts, or degraded performance associated with fringing fields resulting from the inhomogeneous structure between lines. To successfully utilize nanoporous films as interlayer dielectrics, an understanding of the pore size and size distribution is necessary. Furthermore, such information will be invaluable in understanding the pore formation process and developing structure-property relationships.

Despite its importance, pore size distribution has been difficult to accurately measure. Adsorption porosimetry,⁵ in-

volving the measurement of adsorption isotherms of a vapor onto the pore surface, requires judicious selection of the vapor probe, can be complicated by matrix swelling effects, and may not be applicable to closed-cell structures if the vapor does not penetrate into the pores. Positron annihilation lifetime spectroscopy^{6,7} requires a calibration curve to convert the deconvoluted lifetime data into pore size and it has been observed that this technique can be material dependent. Furthermore, the inverse Laplace transform procedure utilized to convert decay data to lifetimes is nontrivial and particular care must be taken in the treatment of the data to minimize the possibility of generating spurious pore size distributions. Quantitative analysis of the pore structure from transmission electron microscopy is complicated by superimposed pores in cross-sectional specimens. Finally, small angle neutron scattering which has been utilized for porous silica,⁸ is not well suited to some important hydrogen-containing nanoporous systems, e.g., porous MSSQ, due to the lack of scattering length density contrast⁹ between the matrix material and the pores.

In this letter, we describe quantitative determination of the pore size distribution in nanoporous low- k films using small angle x-ray scattering (SAXS), where sufficient contrast arises from the electron density difference between MSSQ and air. To produce these films, the MSSQ ($M_w = 15k$, Dow Corning) and the sacrificial organic component, denoted as the porogen, are dissolved in a mutual solvent (e.g., propylene glycol methyl ether), spin coated onto Si substrates, and annealed under a N₂ atmosphere to 450 °C at a ramp rate of 5 °C/min. For these studies, the porogen was a copolymer poly(methyl methacrylate-*co*-dimethylaminoethyl methacrylate), or P(MMA-*co*-DMAEMA), which was synthesized by atom transfer radical polymerization [$M_w = 12k$, PDI = 1.1]. Previous publications have discussed the pore generation process in MSSQ in much greater detail.^{2,10}

Field emission scanning electron microscopy (FESEM) was performed on each of the films using a Hitachi S-4700 scanning electron microscope. Representative cross-sectional

^{a)} Author to whom correspondence should be addressed. Current address: IBM T. J. Watson Research Center, Yorktown Heights, NY 10595; electronic mail: ehuang@us.ibm.com

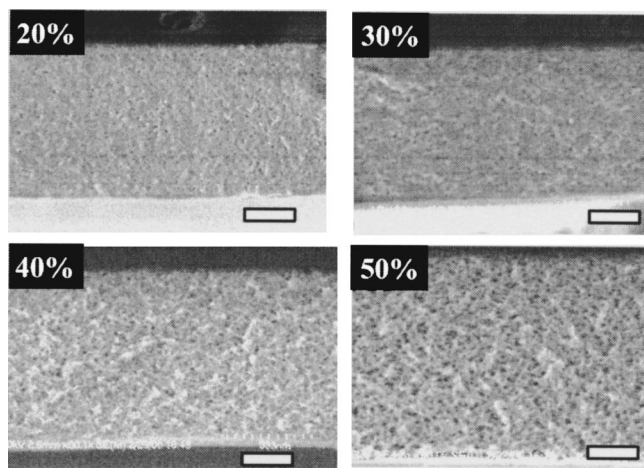


FIG. 1. Field emission scanning electron microscopy (FESEM) images obtained from a cross section of the porous MSSQ films as a function of porosity. Scale bar=200 nm.

images for cleaved films generated from samples with initial porogen loadings ranging from 20 to 50 wt% are shown in Figs. 1(a)–1(d). These high resolution images suggest that the visible pores have diameters of ~ 10 – 20 nm and are uniformly dispersed throughout the thickness of the film. Furthermore, a progressive increase in pore size is observed with increasing porosity (porogen loading). Although FESEM provides useful information regarding the film structure and is relatively easy to perform, the extraction of accurate quantitative values for the pore size and size distribution from these images is difficult. This is due to several primary factors: e.g., fracture induced artifacts and the limitations of the FESEM in resolving smaller pores.

We have utilized SAXS,¹¹ a well-established technique that probes structural correlations for length scales of 1–100 nm. SAXS experiments were performed at the IMM-CAT at the Advanced Photon Source at Argonne National Laboratory. X rays from an undulator were monochromatized with a Ge (111) crystal to an energy of 7.66 keV. Slits confined the beam size to either $100 \times 100 \mu\text{m}$ (high resolution) or $200 \times 200 \mu\text{m}$ (low resolution). An area detector was used with a sample to detector distance of either 2750 mm (high resolution) or 235 mm (low resolution). The samples were positioned with the substrate normal coinciding with the incident beam. To reduce attenuation from the substrate, $\sim 80 \mu\text{m}$ substrates were used with film thicknesses of ~ 0.5 – $0.8 \mu\text{m}$ (which transmitted $\sim 25\%$ of the incident beam). In contrast to real space methods, such as electron microscopy, the information obtained from SAXS measurements is generated over a much larger sampling volume. As a result, the number of pores probed in these experiments is orders of magnitudes larger than for real space techniques and a better statistical representation is attained.

Due to the high flux afforded by the undulator source and sufficient electron density contrast between the two components, measurements were performed on single films and data were typically acquired over ~ 5 – 10 min. Since scattering from such thin films can be inherently weak for some of these systems, great care was used to reduce background scattering. First, double-sided polished wafers were used to eliminate scattering emanating from the substrate roughness.

Parasitic slit scattering from the beam defining slits was minimized through the use of slits with hemispherical polished blades and the careful placement of guard slits. Finally, the sample was placed under vacuum and the placement of windows was limited to a position between the beamstop and the detector and before the beam defining slits. The lack of windows near the sample and the placement of the final window after the beamstop significantly reduces the background scattering.

The SAXS data were background subtracted, circularly averaged, and normalized with respect to the transmitted beam intensity. Data for a series of films where the initial porogen loading ranged from 5–50 wt% are shown by the symbols in Fig. 2(a) and are plotted on a log–log plot as a function the scattering vector, $q = (4\pi/\lambda)\sin(\theta)$, where 2θ is the angle between the scattered photon and transmitted beam. The data sets shows similar characteristics: the scattering is relatively flat at low q and drops off asymptotically at higher q with roughly a q^{-4} dependence. With increasing porosity, the position where the scattered intensity drops off, which is inversely related to the pore size, shifts to lower q , and the overall scattering intensity, which is proportional to the number of pores and the pore volume, increases. Both of these observations are consistent with an increase in pore size with increasing porosity.

To determine the pore size distribution, we have modeled the data using several approximations. First we assume that the pores are spherical, i.e., pore shape is ignored. Second, the hard sphere exclusion radius is assumed to be equivalent to the pore size, i.e., there is no depletion layer. Third, we approximate the interference due to inter-pore scattering with an approach described by Pedersen, using a hard sphere model and an approximation that the pores are locally monodisperse in size.¹² Because there is a broad distribution of cluster sizes (vide infra), both of these approximations are valid as long as the pores are largely not interconnected. The high porosity films are discussed below. The scattered intensity, $I(q)$, is written as

$$I = c \int_0^\infty n(r)f(qr)S(qr)dr,$$

where c is a constant, $n(r)$ is the pore size distribution, $f(qr)$ is the spherical form factor, and $S(qr)$ is the structure factor for the monodisperse hard sphere model.¹³

We have considered several types of pore size distributions and found that the SAXS data are best modeled using a log-normal pore size distribution

$$n(r) = \frac{1}{(2\pi)^{0.5}r_0\sigma \exp(0.5\sigma^2)} \exp\left\{-\frac{[\ln(r/r_0)]^2}{2\sigma^2}\right\},$$

where r is the pore radius, r_0 is the pore radius corresponding to the maxima of the distribution, σ is related to the width of the distribution, and $n(r)$ is the number fraction with pore radius r . The good fit for the log-normal distribution is not surprising as this has been observed in a variety of other growth processes.^{14,15}

Fits to the data are shown for each of the data sets in Fig. 2(a) (solid lines) and the distributions generated from these fits are displayed in Fig. 2(b). Generally, the fits were performed to closely match a large region in q near the drop off

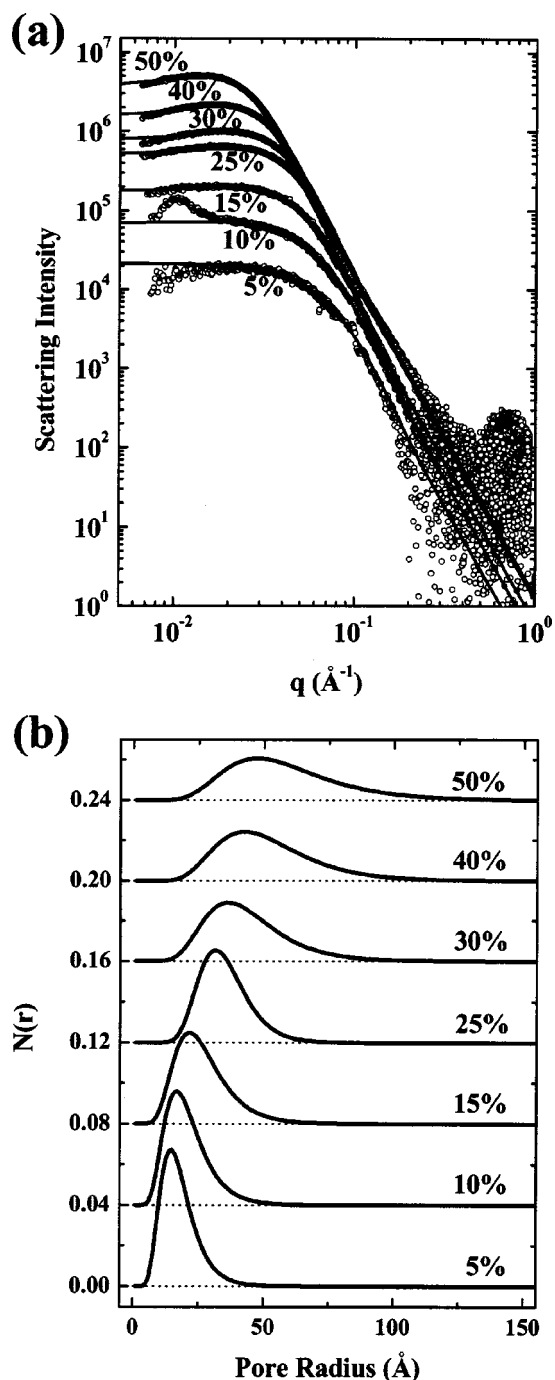


FIG. 2. (a) Circularly averaged scattering intensity (symbols) and fits (solid lines) vs q and (b) size distribution generated from the model fits. The bump at low Q for the 15% film is due to imperfect subtraction of slit scattering.

in intensity. The scattering vector corresponding to this position, denoted as q^* , is approximately equal to $\pi/2r$, where r is the radius of the pores. Thus, the data in the q range near q^* is of most relevance. At lower q , some deviations between the data and fits are observed; this is attributed to difficulties in modeling pore-pore correlations in the system. Of particular note is the lack of fringes in the scattering data that are inherent in the spherical form factor [$f(qr)$] and are

normally observed in well-defined systems. The absence of these fringes immediately shows that there is a relatively broad pore size distribution as any interference in the scattering data, normally associated with monodisperse systems, is smeared out. The size distributions in Fig. 2(b) show that the average pore size increases and the size distribution broadens with increasing porosity. This is in good qualitative agreement with the images obtained by FESEM. Furthermore, estimates of the pore size obtained from the FESEM images are consistent with the pore size distributions generated by SAXS. These results show that for this particular material set, the pore sizes are sufficiently small relative to device feature sizes. Although this treatment is based on a morphology comprised of nearly spherical pores, treatment of the higher porosity samples, which have an interconnected structure, produced values that still correlate well with FESEM images. At higher porosities, the bicontinuous pore structure becomes difficult to define; consequently, the structure factor for such a morphology is difficult to model. For a rigorous treatment of interconnected systems, the structure factor must be modified to account for the deviation in morphology. The applicability of other models^{16–18} for open-celled nanoporous films is currently under investigation.

Use of the Advanced Photon Source was supported by the U.S. Department of Energy, Office of Science, Office of Basic Energy Sciences, under Contract No. W0-31-109-ENG-38. The SAXS experiments were performed on the IMM-CAT beamline 8-ID. Program funding was provided by the NIST-ATP cooperative agreement No. 70NANB8H4013.

- ¹ Y. Charlier, J. L. Hedrick, T. P. Russell, A. Jonas, and W. Volksen, *Polymer* **36**, 987 (1995).
- ² J. L. Hedrick, R. D. Miller, C. J. Hawker, K. R. Carter, W. Volksen, D. Y. Yoon, and M. Trollsas, *Adv. Mater.* **10**, 1049 (1998).
- ³ R. H. Baney, M. Itoh, A. Sakakibara, and T. Suzuki, *Chem. Rev.* **95**, 1409 (1995).
- ⁴ S. J. Martin, J. P. Godschalx, M. E. Mills, E. O. Shaffer, and P. H. Townsend, *Adv. Mater.* **12**, 1769 (2000).
- ⁵ M. R. Baklanov, K. P. Mogilnikov, V. G. Polovinkin, and F. N. Dultsev, *J. Vac. Sci. Technol. B* **18**, 1385 (2000).
- ⁶ D. W. Gidley, W. E. Frieze, T. L. Dullo, A. F. Yee, E. T. Ryan, and H.-M. Ho, *Phys. Rev. B* **60**, R5157 (1999).
- ⁷ M. P. Petkov, M. H. Weber, K. G. Lynn, K. P. Rodbell, and S. A. Cohen, *J. Appl. Phys.* **86**, 3104 (1999).
- ⁸ W.-I. Wu, W. E. Wallace, E. K. Lin, G. W. Lynn, C. J. Glinka, E. T. Ryan, and H.-M. Ho, *J. Appl. Phys.* **87**, 1193 (2000).
- ⁹ G. Yang, R. M. Briber, E. Huang, H.-C. Kim, P. Rice, R. D. Miller, and W. Volksen, *Appl. Phys. Lett.* (in press).
- ¹⁰ C. V. Ngyuen, K. R. Carter, C. J. Hawker, J. L. Hedrick, R. L. Jaffe, R. D. Miller, J. F. Remenar, H.-W. Rhee, P. Rice, M. F. Toney, M. Trollsas, and D. Y. Yoon, *Chem. Mater.* **11**, 3080 (1999).
- ¹¹ A. Guinier, G. Fournet, C. B. Walker, and K. L. Yudowitch, *Small-Angle X-Ray Scattering* (Wiley, New York, 1955).
- ¹² J. S. Pedersen, *J. Appl. Crystallogr.* **27**, 595 (1994).
- ¹³ D. J. Kinning and E. J. Thomas, *Macromolecules* **17**, 1712 (1984).
- ¹⁴ K. O'Grady and A. Bradbury, *J. Magn. Magn. Mater.* **39**, 91 (1983).
- ¹⁵ J. Soderlund, L. B. Kiss, G. A. Niklasson, and C. G. Granqvist, *Phys. Rev. Lett.* **80**, 2386 (1998).
- ¹⁶ N. F. Berk, *Phys. Rev. Lett.* **58**, 2718 (1987).
- ¹⁷ S.-H. Chen, D. Lee, and S.-L. Chang, *J. Mol. Struct.* **296**, 259 (1993).
- ¹⁸ H. Jinnai, T. Hashimoto, D. Lee, and S.-H. Chen, *Macromolecules* **30**, 130 (1997).